POLITECNICO DI TORINO
Repository ISTITUZIONALE

Improvement of instrumented indentation test accuracy by data augmentation with electrical contact resistance

*Original*
Improvement of instrumented indentation test accuracy by data augmentation with electrical contact resistance / Galetto, M., Kholkhujaev, J., Maculotti, G.. - In: CIRP ANNALS. - ISSN 0007-8506. - ELETTRONICO. - 72:1(2023), pp. 469-472. [10.1016/j.cirp.2023.03.034]

*Availability:*
This version is available at: 11583/2979082 since: 2023-06-05T06:23:25Z

*Publisher:*
Elsevier

*Published*
DOI:10.1016/j.cirp.2023.03.034

*Terms of use:*

This article is made available under terms and conditions as specified in the corresponding bibliographic description in the repository

*Publisher copyright*

(Article begins on next page)

08 October 2026

CIRP Annals - Manufacturing Technology 72 (2023) 469–472

Contents lists available at ScienceDirect

CIRP Annals - Manufacturing Technology

journal homepage: https://www.editorialmanager.com/CIRP/default.aspx

# Improvement of instrumented indentation test accuracy by data augmentation with electrical contact resistance

Maurizio Galetto (2)[a,*], Jasurkhuja Kholkhujaev[a,b], Giacomo Maculotti[a]

[a] Department of Management and Production Engineering, Politecnico di Torino, Corso Duca degli Abruzzi 24, 10129 Torino, Italy
[b] Turin Polytechnic University in Tashkent, Kichik Halka Yuli, 17, Tashkent, Uzbekistan

ARTICLE INFO

*Article history:*
Available online 28 April 2023

*Keywords:*
Nano indentation
Calibration
Electrical contact resistance

ABSTRACT

Instrumented Indentation Test allows thorough surface multi-scale mechanical characterisation by depth-sensing the indenter penetration and correlating it with the indenter-sample contact area and the applied force. Localised plastic phenomena at the indentation edge, i.e. pile-up and sink-in, may bias the characterisation results. Current approaches attempt correcting related systematic errors by numerical simulation and AFM-based techniques. However, they require careful tuning and complex and expensive experimental procedures. This work proposes a methodology based on in-situ Electric Contact Resistance which augments information on the contact area and allows edge effect correction. The methodology is demonstrated and validated on industrially relevant metallic materials.

© 2023 CIRP. Published by Elsevier Ltd. All rights reserved.

## 1. Introduction

Current industrial trends within the Green Deal are pushing the development of materials, manufacturing process and quality inspection to support the green transition [1]. As far as surface technologies are concerned, coatings and nano-structuring are extensively studied to enhance technological surface properties in various applications [2]. For example, the manufacturing of Ge coating for photovoltaic panels is studied to replace current solutions thanks to the higher energy efficiency of Ge [3]. E-mobility applications benefit from thin multi-layer coatings and nano-structuring of battery electrodes' surfaces to improve their durability, performance and efficiency [4]. Composites coatings extend components' durability by enhancing the resistance to harsh environments and by engineering mechanical and tribological properties to minimise wear while extending service life and optimising performances [5]. Also, more conventional manufacturing processes are still being optimised to induce surface modification capable of extending the life of components, e.g. by introducing residual stresses that can increase resistance to fatigue and killer notches [6].

Indeed, adequate quality inspection techniques are required to evaluate the effectiveness of manufacturing processes and the properties of materials. Amongst them, Instrumented Indentation Test (IIT) can evaluate a wide range of mechanical properties of a surface at different characterisation scales, ranging from nano to macro range, with limited sample preparation [7]. In the macro range, IIT can replace conventional destructive tests. At micro- and nano-range, IIT allows the local evaluation of mechanical properties, e.g. mapping and quantitatively distinguishing and characterising phases, and of micro- and nano-structures, and allows measuring mechanical properties of coatings in-depth without cross-sectioning the samples [5,7].

IIT consists of applying a loading-holding-unloading force-controlled cycle with an indenter on a sample to be characterised. During the test, the applied force, $F$, and the indenter penetration depth in the sample, $h$, are measured, see, e.g., Fig. 1.

IIT is a depth-sensing technique, and the calibrated relationship between the indenter penetration depth and the area of the contact surface between the indenter and the material, $A_p(h)$, allows resolving characterisation at shallow depths, thus overcoming limits of conventional hardness tests. Analysing the indentation curve allows evaluating mechanical properties, e.g. the indentation hardness, $H_{IT}$, and the indentation modulus, $E_{IT}$, which estimates the Young's modulus of the tested material, as:

$$H_{IT} = \frac{F}{A_p(h_c)} \tag{1}$$

$$E_{IT} = \frac{1-\nu_s^2}{\frac{2\sqrt{A_p(h_{c,max})}}{S\sqrt{\pi}} - \frac{1-\nu_i^2}{E_i}} \tag{2}$$

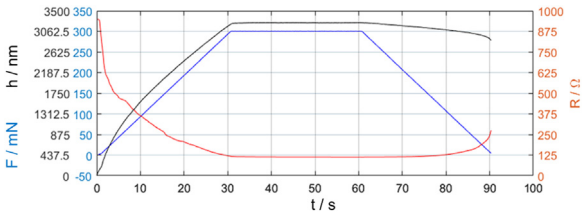


**Fig. 1.** Force, penetration depth and electrical resistance as a function of test time. Notice the continuous decrease of the measured resistance for increasing contact. Indentation on Al sample.

* Corresponding author.
*E-mail address:* maurizio.galetto@polito.it (M. Galetto).

https://doi.org/10.1016/j.cirp.2023.03.034
0007-8506/© 2023 CIRP. Published by Elsevier Ltd. All rights reserved.

where $\nu_i$ and $E_i$ are the indenter Poisson and Young's modulus, $h_c$ is the corrected indenter penetration depth, as per Eq. (3), for the zero-contact point displacement, $h_0$, the elastic displacement of the frame, $C_f F$, which is proportional to the frame compliance $C_f$, and for the elastic recovery of the material, $\varepsilon \frac{F}{S}$, which is proportional to the reciprocal of the contact stiffness $S$ of the sample, and to a factor $\varepsilon$ related to the indenter geometry, typically 0.75 for Berkovich indenters:

$$h_c = h - h_0 - \varepsilon \frac{F}{S} - C_f F \tag{3}$$

$S$ is derived, according to Eq. (4), from the empirical evaluation of the measured contact stiffness, $S_m$, at the onset of the unloading, i.e. at maximum force $F_{max}$ and penetration $h_{max}$ and the calibrated value of the frame compliance $C_f$:

$$C_{tot} = \frac{1}{S_m} = \left( \frac{\partial F}{\partial h}\bigg|_{h_{max}} \right)^{-1} = C_f + \frac{1}{S} \tag{4}$$

Calibration is essential to establish traceability and correct systematic errors, providing end users with confidence in the characterisation results. $C_f$ calibration corrects systematic errors due to elastic displacement of the instrument, and $A_p(h)$ calibration corrects systematic errors due to the deviation from the nominal indenter geometry. In the most general case, for a Vickers or a Berkovich indenter, $A_p(h)$ is a polynomial function with several terms catering for the tip dihedral angle and geometric errors, e.g. tip rounding and imperfections [8]. However, despite this calibration, further bias in the $A_p(h)$ can be present due to local plasticity at the indentation edge. This phenomenon consists in the material either piling up or sinking in around the indenter (see Fig. 2): in the former case, the calibrated $A_p(h)$ systematically underestimates the actual contact area; in the latter, $A_p(h)$ overestimates it, resulting in systematic errors in the $H_{IT}$ that are inverse to the error and in nonlinear trends in the $E_{IT}$ [9]. The edge effect depends on the ratio between the yield stress and the Young's modulus, and on the work-hardening coefficient of the tested material [9]. Edge effect error is critical in the large nano-range and in the micro-range, whilst it is typically negligible in the macro-range, as the indentation size is significantly larger than the error introduced [10]. A consistent amount of literature has proposed correction methods. They are either based on post-indentation analysis of the indentation by AFM, which requires complex empirical setup and non-trivial assumption to manage elastic recovery in the material [11], or on numerical approaches, which rely on complex modelling of the system and the material behaviour [12].

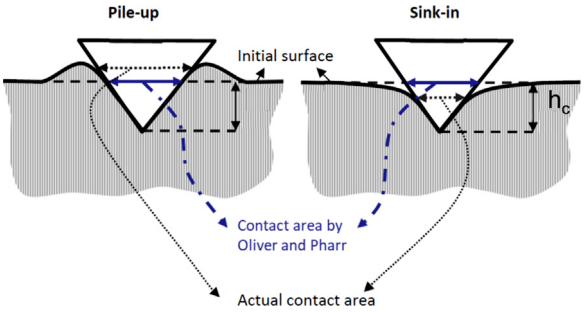


**Fig. 2.** Pile-up and Sink-in edge effect bias estimation of projected contact area by the conventional Oliver and Pharr approach [7], which respectively underestimates and overestimates the actual area.

IIT data augmentation by in-situ Electrical Contact Resistance (ECR) allows the evaluation of the electromechanical properties of tested materials. ECR, using a doped diamond indenter, enables the measurement of the continuous variation of the resistance by applying a current across the indentation contact and measuring the resulting voltage as the applied force varies, see Fig. 1. Electrical signal variations have been exploited to identify phase change transformation induced by high stress, crucial to engineering semiconductors manufacturing [13], characterise materials behaviours [14], and study contact mechanics and plasticity at nano-scale [15].

This work proposes a methodology based on an experimental setup and physics modelling that relies on ECR data augmentation of IIT to correct systematic errors due to the edge effect in the $A_p(h_c)$ measurement. Section 2 will describe the proposed methodology, Section 3 the case study used for validating and demonstrating the proposed methodology on industrially relevant metallic materials and Section 4 will draw conclusions.

## 2. ECR-based correction of edge effect systematic errors

### 2.1. Fundamentals of ECR

According to the ECR framework [16], the relationship between the electrical resistance and the contact area can be written as:

$$R = R_c + R_s + R_{tip} + R_{electronics} = \frac{C_1}{A_p} + \frac{C_2}{\sqrt{A_p}} + R_0 \tag{5}$$

The resulting electrical resistance $R$ depends on the contact resistance $R_c$, inversely proportional to the contact area $A_p$ with a material-dependent constant $C_1$ (predominant at contact onset [16]), and on the spreading resistance $R_s$, inversely proportional to the square root of the contact area with a constant $C_2$, depending on the sample and the indenter system resistivity and on the contact geometry [16]. An offset term $R_0$ is included, modelling the system resistance contribution of the tip resistance ($R_{tip}$) and the electronics and system resistance ($R_{electronics}$) [16].

This fundamental relationship has been sparsely exploited in the most recent nanoindentation literature to obtain measurements of the area. However, all the proposed methods either rely on convoluted mathematical procedures, not easily applicable [17], or on using expensive calibration materials, i.e. Au, Cu [18,19]. Furthermore, the use of ECR for improving the metrological properties of the mechanical characterisation is neglected nor used to increase the measurement quality (i.e., precision and/or accuracy).

### 2.2. Methodology for correcting edge effect

The proposed methodology exploits Eq. (5), which can be rewritten to isolate the contact area as follows:

$$A_p(R) = \frac{C_3}{\sqrt{R}} + \frac{C_4}{R^2} + C_5 \tag{6}$$

where parameters $C_3$, $C_4$ and $C_5$ can be estimated by regression using experimental data. Eq. (6) allows evaluating the contact area by avoiding the penetration depth measurement, which may be biased by the edge effects, thus achieving an accurate measurement of the actual contact area. The regression dataset can be collected by performing replicated indentations at different levels of force by an indentation platform for which $C_f$ and $A_p(h_c)$ have been formerly calibrated [8], and measuring $F_{max}$, $h_{c,\max}$ and $R(h_{c,\max})$. An Orthogonal Distance Regression (ODR) is exploited to estimate the parameters of Eq. (6) since ODR allows more robust results than ordinary least-square regression (LSQ) when the uncertainty in regressor variables, i.e., in the case at hand, the resistance, is not negligible [8]. Indeed, the dependent variable $A_p(R)$ has to be estimated basing on the formerly calibrated relationship $A_p(h_c)$ and exploiting unbiased measurements of $h$. Thus, data must be gathered in a range of applied force in which the material does not suffer of the edge effect. However, this behaviour is typically located in the flat part of the curve expressed by Eq. (6). Hence, when the ODR is applied to experimental data gathered in this part of the curve, this flat trend may induce poor robustness in the prediction for the whole range of variation of $R$, see also Fig. 5. Therefore, Eq. (6) parameters cannot be computed directly from data collected on the material needing the edge effect correction. Conversely, the proposed approach relies on the use of a reference material, which is not affected by edge effects at the scale level at which the Eq. (6) is used, i.e. nano- and micro-range. This condition can be satisfied by typical hardness reference materials, e.g. Aluminium and Brass.

Though, since the estimated parameters are correlated to the calibration material resistivity, a "normalisation" to rescale the effect of material resistivity is required to apply the resistance-based evaluation of the area on the material needing edge effect correction. Considering the order of magnitude of the parameters $C_1$ and $C_2$ of Eq. (5) for metals and semiconductors, and of the area when $h_c > 20$ nm, Eq. (5) can be approximated as [16,19]:

$$\Delta R = R - R_0 \approx \frac{C_2}{\sqrt{A_p}} \tag{7.1}$$

from which the following approximation is obtained:

$$A_p(\Delta R) \approx \frac{C_4}{\Delta R^2} \tag{7.2}$$

Let quantities pertaining to the reference material and the material needing correction be indicated with subscript $m_R$ and $m_C$ respectively, and with "*" the quantities evaluated in conditions unaffected by the edge effect. Let the data be collected and evaluate Eq. (6) on the reference materials, i.e. $A_{p,m_R}(R)$. Then, for the material needing correction, in conditions not affected by the edge effect, in a neighbourhood of $\Delta R^*_{m_C}$ (*i.e.* $\Delta R^*_{m_C} \pm \delta R$), and applying the resistivity rescaling, the corrected contact area is:

$$A_{p,m_C,corr}\left(\Delta R^*_{m_C} \pm \delta R\right) = A_{p,m_R}\left(\Delta R^*_{m_C} \pm \delta R\right) \frac{A_{p,m_C}\left(h^*_{c,m_C}\right)}{A_{p,m_C}\left(\Delta R^*_{m_C}\right)} \tag{8}$$

Eq. (8) is exploited to robustly evaluate the regression parameters of Eq. (6) for the $m_C$, by a Monte Carlo Markov Chain (MCMC) [20]. The MCMC assumes a gaussian process [21] for the $A_p \sim GP\left(A_{p,m_C,corr}(R), N(0,\Sigma_A)\right)$, with the deterministic part as per Eq. (8), and the stochastic contribution (included in the covariance matrix $\Sigma_A$) with the variance estimated from the reproducibility of $A_p$ and $R$ [21]. In the neighbourhood of each measured $(F_{max}, h_c, \Delta R)^*_{m_C}$, additional data are randomly extracted based on the MCMC model, and the obtained larger data set is exploited to fit the regression model to accurately estimate area. The uncertainty of the corrected area is estimated according to GUM [22], propagating the standard deviation of the estimated parameters, the RMSE of the residuals and the standard uncertainties of the regressors. Intuitively, the MCMC approach allows increasing the data set numerosity while providing a known correlation based on the physical relationship between the area and the resistance, as per Eq. (8). This introduces a local trend in the data which compensates for the flatness of the $A_{p,m_C}(R)$ in the region that is exploited for estimating the regression parameters of Eq. (6), see also Fig. 5.

## 3. Case study

### 3.1. Experimental setup

Three materials are considered: Aluminium (Al), Brass (BR) - not affected by pile-up - and stainless steel (SS), requiring the pile-up correction. Samples were calibrated by macro-IIT, scale at which edge effects are negligible [8], with a macro-IIT indentation platform AXHU-09 by AXIOTEK, calibrated by INRiM and hosted in the Mind4Lab of Politecnico di Torino. Table 1 shows the results of the calibration.

**Table 1**
Results of $H_{IT}$ calibration with macro-IIT: mean and uncertainty at 95% confidence level.

| Material | Al | BR | SS |
|---|---|---|---|
| $H_{IT}$ / GPa | 1.117±0.028 | 0.878±0.022 | 8.127±0.203 |

A state-of-the-art Anton Paar MCT$^3$ STeP6 indentation platform is exploited in this work to demonstrate and validate the methodology proposed in Section 2.2. The platform is equipped with a doped-diamond conductive Berkovich indenter and calibrated force transducer, with an uncertainty of 0.5 mN, and LVDT displacement sensor, with an uncertainty of 0.6%. The frame compliance and the area shape function of the indenter are calibrated as per the standard approach [8]. In-house prototyping to support ECR was developed, see Fig 3. Experiments are performed in the range from 1 N to 30 N. The application considers the Al as reference material to calibrate the method, BR for validation, as it is not affected in the considered range by pile-up, and SS for demonstrating the edge effect correction.

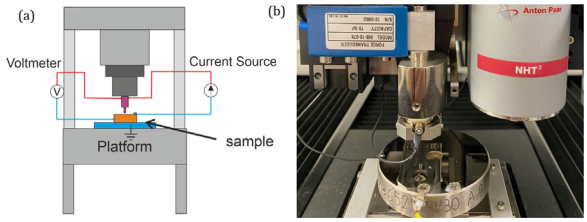


**Fig. 3.** (a) Scheme of the ECR setup. (b) Experimental setup with state-of-the-art Anton Paar MCT$^3$ and NHT$^3$ prototyped to support the ECR data augmentation in the Mind4-Lab of DIGEP-PoliTO.

Additionally, with a calibrated nanoindenter Anton Paar NHT$^3$ with a Berkovich indenter, data were collected to show an extended trend of the $H_{IT}$. This shows the evolution from the Indentation Size Effect zone (ISE), at the lower end of the nano-range (see the left side of Fig. 4), through a constant unbiased range (see the centre of Fig. 4), to the onset of a systematic trend at $F > 10$ N, evidence of pile-up (for the SS) (see right side of Fig. 4).

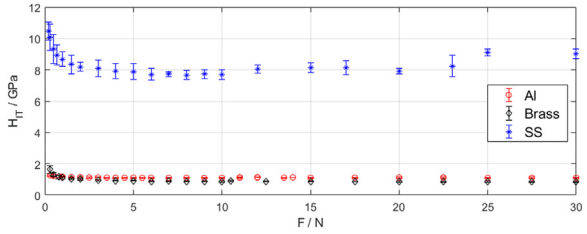


**Fig. 4.** Through scale $H_{IT}$ trend of the three considered materials. At the low forces, notice ISE. At high loads, notice the systematic trend indicating pile-up for SS, which is not present for the Al and BR. For the three materials, notice a constant unbiased range in the central part of the plot.

### 3.2. Method setup and validation

The methodology presented in Section 2.2 is applied to the three materials: Fig. 5(a) shows the collected data for the three materials, qualitatively in agreement with the trend of Eq. (6), and with differences induced by electromechanical response specific to each material. The Eq. (6) parameters are estimated by ODR exploiting data on Al, yielding an RMSE of 4.9e-10 m$^2$ and an $R^2$ of 0.9946. Method validation is performed on Brass, as it allows verification against an unbiased condition. Rescaling according to Eq. (8) is performed: 100 data points are generated by the MCMC in a neighbourhood $\delta R = 0.5\ \Omega$ of the experimental raw data and exploited to evaluate the model of Eq. (6) for Brass.

Results in Fig. 5(b) show that, at a 95% confidence level, there are no systematic differences between the estimated trend of $A_{p,BR,corr}$ and raw data. Moreover, the proposed approach results in a smaller

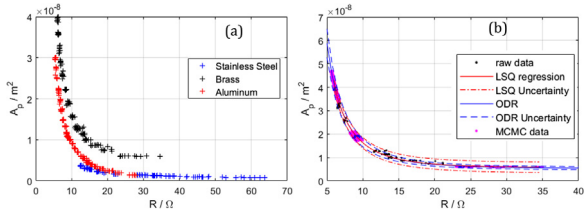


**Fig. 5.** (a) ECR raw data collected on the three materials: notice the common trend, shifted in the $A_p$-R space due to the different material electromechanical response. (b) Results of method validation on Brass: with respect to LSQ regression (red) applied to raw data (black), the ODR regression (blue) applied to the MCMC-generated data (magenta) achieves a more precise estimation, compatible with both LSQ and raw data.

measurement uncertainty than an ordinary least-square regression. The effect of the experimental points $(F_{max}, h_c, R)^*_{m_C}$ to apply the methodology is evaluated, thanks to the unbiased measurement on Brass. Random extractions from the whole BR dataset are performed considering varying subsample size, from 3 to 10 load levels, and no systematic differences in the estimated trend can be highlighted.

### 3.3. Edge effect correction

The methodology is finally applied to the SS data, which show a systematic increase of the $H_{IT}$ at high levels of force. Data normalisation, MCMC setup and ODR are applied to the data not affected by significant pile-up, i.e. for $F<10$ N, see Fig. 4. Fig. 6 shows the results and compares the effectiveness and the necessity of the data rescaling and of the MCMC with respect to the simple application of the ODR on the data unaffected by pile-up, i.e. the horizontal asymptotic region of $A_p(R)$.

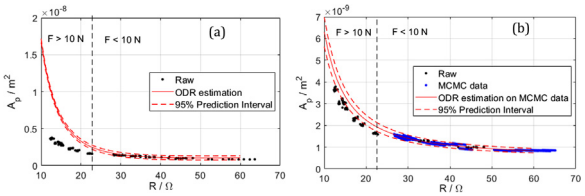


**Fig. 6.** Prediction of corrected area on pile-up affected material (SS) based on (a) ODR applied to raw data and (b) MCMC data. Notice the consistent identification of pile-up affected data from the vertical line, inferred from Fig. 3 and the data out of the prediction bound of the ODR (red-dashed line).

The method successfully identifies systematic errors in data at $F>10$ N at 95% confidence interval, and the effect of the correction is assessed on the evaluation of the $H_{IT}$ at different levels of $F_{max}$ (see Fig. 7) and comparing it with the calibrated value in Table 1, showing the successful application of the method (the average relative error is 7% and is not statistically significant). Indeed, the systematic correction comes with the cost of increased uncertainty, worsening from 4% to 7%. The method was compared with some alternatives available in the literature. Park's method requires a-priori knowledge of $E$ [23] and yields a severe bias (223%) and a larger uncertainty (19%) with respect to the proposed ECR-based method. Conversely, Pharr et al.'s method, based on characteristic lengths scale for ISE correction [24], allows better accuracy (3%) with 10% relative uncertainty: the prediction of Pharr et al.'s [24] and of the ECR-based approach are not statistically different, and the latter is more precise thanks to the data augmentation.

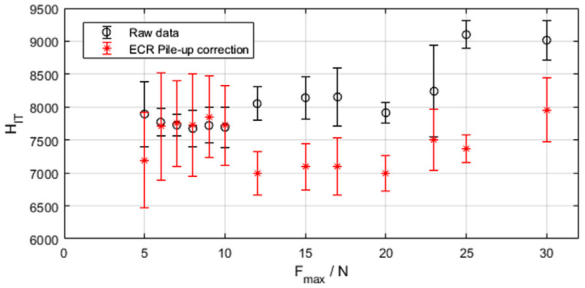


**Fig. 7.** Effect of ECR-based pile-up correction according to the proposed methodology on the $H_{IT}$. Results on SS. Notice the effective removal of the systematic errors at $F >$ 10 N.

## 4. Conclusions

Local plasticity introduced by the edge effect biases the area measurement and, consequently, the characterisation results of Instrumented Indentation Test. This work presented a correction method for the edge effect based on data augmentation obtained by in-situ Electrical Contact Resistance (ECR) measurement. With respect to other solutions available in the literature, it does not require additional expensive measurements to be performed by AFM or convoluted mathematical approaches but is only applicable to conductive materials. Conversely, it relies on a data-driven approach based on physics modelling, and it was validated and demonstrated on industrially relevant materials showing an effective correction of edge effect with the cost of a marginal increase of measurement uncertainty. Future work will address the application to nano-scale and nanomaterials and the method validation by numerical multi-scale and multi-physics modelling. Also, the formalisation of the comparison of available correction methods will be reported.

## Declaration of Competing Interest

The authors declare that they have no known competing financial interests or personal relationships that could have appeared to influence the work reported in this paper.

## References

[1] Wolf S, Teitge J, Mielke J, Schütze F, Jaeger C (2021) The European Green Deal — More Than Climate Neutrality. *Intereconomics* 56:99–107.
[2] Bruzzone AAG, Costa HL, Lonardo PM, Lucca DA (2008) Advances in Engineered Surfaces for Functional Performance. *CIRP Annals* 57:750–769.
[3] Patel M, Karamalidis AK (2021) Germanium: A Review of its Us Demand, Uses, Resources, Chemistry, and Separation Technologies. *Separation and Purification Technology* 275:118981.
[4] Chow G, Uchaker E, Cao G, Wang J (2015) Laser-Induced Surface Acoustic Waves: An Alternative Method to Nanoindentation for the Mechanical Characterisation of Porous Nanostructured Thin Film Electrode Media. *Mechanics of Materials* 91:333–342.
[5] Bouzakis KD, Michailidis N, Skordaris G, Bouzakis E, Biermann D, M'Saoubi R (2012) Cutting with Coated Tools: Coating Technologies, Characterisation Methods and Performance Optimisation. *CIRP Annals* 61:703–723.
[6] Meijer AL, Stangier D, Tillmann W, Biermann D (2022) Induction of Residual Compressive Stresses in the Sub-Surface by the Adjustment of the Micromilling Process and the ToolS Cutting Edge. *CIRP Annals* 71:97–100.
[7] Lucca DA, Herrmann K, Klopfstein MJ (2010) Nanoindentation: Measuring Methods and Applications. *CIRP Annals* 59:803–819.
[8] Galetto M, Genta G, Maculotti G (2020) Single-Step Calibration Method for Nano Indentation Testing Machines. *CIRP Annals* 69:429–432.
[9] Cheng YT, Cheng CM (1998) Effects of 'Sinking in' and 'Piling Up' on Estimating the Contact Area Under Load in Indentation. *Philosophical Magazine Letters* 78:115–120.
[10] Kholkhujaev J, Maculotti G, Genta G, Galetto M (2023) Calibration of Machine Platform Nonlinearity in Instrumented Indentation Test in the Macro Range. *Precision Engineering* 81:145–157.
[11] Moharrami N, Bull SJA (2014) A Comparison of Nanoindentation Pile-Up in Bulk Materials and Thin Films. *Thin Solid Films* 572:189–199.
[12] Pöhl F, Huth S, Theisen W (2014) Indentation of Self-Similar Indenters: An FEM-Assisted Energy-Based Analysis. *Journal of the Mechanics and Physics of Solids* 66:32–41.
[13] Pharr G, Oliver WC, Cook RF, Kirchner PD, Kroll MC, Dinger TR, Clarke DR (1992) Electrical Resistance of Metallic Contacts on Silicon and Germanium During Indentation. *Journal of Materials Research* 7:961–972.
[14] Shastry VV, Ramamurty U (2013) Simultaneous Measurement of Mechanical and Electrical Contact Resistances During Nanoindentation of NiTi Shape Memory Alloys. *Acta Materialia* 61:5119–5129.
[15] Yunus EM, McBride JW, Spearing SM (2009) The Relationship Between Contact Resistance and Contact Force on Au-Coated Carbon Nanotube Surfaces Under Low Force Conditions. *IEEE Transactions on Components, Packaging and Manufacturing Technology* 32:650–657.
[16] Sprouster DJ, Ruffell S, Bradby JE, Stauffer DD, Major RC, Warren OL, Williams JS (2014) Quantitative Electromechanical Characterisation of Materials Using Conductive Ceramic Tips. *Acta Materialia* 71:153–163.
[17] Fang L, Muhlstein CL, Romasco AL, Collins JG, Friedman LH (2009) Augmented Instrumented Indentation Using Nonlinear Electrical Contact Current-Voltage Curves. *Journal of Materials Research* 24:1820–1832.
[18] Comby-Dassonneville S, Volpi F, Parry G, Pellerin D, Verdier M (2019) Resistive-Nanoindentation: Contact Area Monitoring by Real-Time Electrical Contact Resistance Measurement. *MRS Communications* 9:1008–1014.
[19] Volpi F, Rusinowicz M, Comby-Dassonneville S, Parry G, Boujrouf C, Braccini M, Pellerin D, Verdier M (2021) Resistive-Nanoindentation on Gold: Experiments and Modeling of the Electrical Contact Resistance. *Review of Scientific Instruments* 92:035102.
[20] JCGM 101 Evaluation of Measurement Data - Supplement 1 to the "Guide to the Expression of Uncertainty in Measurement" - Propagation of Distributions Using a Monte Carlo Method. 2008, JCGM, Sèvres, France.
[21] Maculotti G, Genta G, Quagliotti D, Galetto M, Hansen HN (2022) Gaussian Process Regression-Based Detection and Correction of Disturbances in Surface Topography Measurements. *Quality and Reliability Engineering International* 38:1501–1518.
[22] JCGM100: Evaluation of Measurement Data — Guide to the Expression of Uncertainty In Measurement (GUM) 2008, JCGM, Sèvres, France.
[23] Park MS (2016) Correction of the Hardness Measurement for Pile-Up Materials with a Nano Indentation Machine. *J Korea Acad Coop Soc* 17:98–106.
[24] Pharr GM, Herbert EG, Gao Y (2010) The Indentation Size Effect: A Critical Examination of Experimental Observations and Mechanistic Interpretations. *Annual Review of Materials Research* 40:271–292.